Chemical ordering in Cr_{3}Al and relation to semiconducting behavior

Z. Boekelheide, D. A. Stewart, and F. Hellman

Phys. Rev. B **86**, 085120 — Published 15 August 2012

DOI: 10.1103/PhysRevB.86.085120

Chemical ordering in Cr_3Al and relation to semiconducting behavior

Z. Boekelheide,[1,2,*] D. A. Stewart,[3] and F. Hellman[1,2]

[1] *Department of Physics, University of California, Berkeley, Berkeley, California 94720, USA*
[2] *Materials Sciences Division, Lawrence Berkeley National Laboratory, Berkeley, California 94720, USA*
[3] *Cornell Nanoscale Facility, Cornell University, Ithaca, New York 14853 USA*

(Dated: June 19, 2012)

Cr_3Al shows semiconductor-like behavior which has been attributed to a combination of antiferromagnetism and chemical ordering of the Cr and Al atoms on the bcc sublattice. This article presents a detailed theoretical and experimental study of the chemical ordering in Cr_3Al. Using density functional theory within the Korringa Kohn Rostoker (KKR) formalism, we consider five possible structures with the Cr_3Al stoichiometry: bcc solid solution, two phase $C11_b$ Cr_2Al + Cr, off-stoichiometric $C11_b$ Cr_3Al, $D0_3$ Cr_3Al, and X-phase Cr_3Al. The calculations show that the chemically ordered, rhombohedrally distorted X-phase structure has the lowest energy of those considered, and should therefore be the ground state found in nature, while the $D0_3$ structure has the highest energy and should not occur. While KKR calculations of the X-phase indicate a pseudogap in the density of states, additional calculations using a full potential linear muffin tin orbital approach and a plane wave technique show a narrow band gap. Experimentally, thin films of $Cr_{1-x}Al_x$ were grown and concentration, growth temperature, and substrate were varied systematically. The peak resistivity (2400 $\mu\Omega$-cm) is found for films with $x = 0.25$, grown epitaxially on a 300°C MgO substrate. At this x, a transition between nonmetallic and metallic behavior occurs at a growth temperature around 400°C, which is accompanied by a change in chemical ordering from X-phase to $C11_b$ Cr_3Al. These results clarify the range of possible structures for Cr_3Al and the relationship between chemical ordering and electronic transport behavior.

I. INTRODUCTION

Alloys and compounds made of metallic elements are generally expected to be metallic, and indeed most are. However, some such compounds are semiconducting or semimetallic, such as $RuAl_2$ and Fe_2VAl.[1] In theory, any compound with an even number of valence electrons in the primitive unit cell can be semiconducting because the electrons can completely fill the valence band. Transition metals usually have several overlapping *d*-like bands at the Fermi energy (E_F) so even in compounds with an even number of electrons typically several bands are partially filled. For an intermetallic compound to be semiconducting, hybridization must shift the bands in a fortuitous way, leaving a gap at E_F.

When intermetallic compounds do have a gap at E_F, they are the subject of significant study. The gap can be exploited for applications, for example, intermetallic semiconductors are attractive for thermoelectric devices due to their typically small gaps and large Seebeck coefficients (ex. ZrNiSn).[2,3] In ferro- or ferrimagnetic compounds, the gap is generally asymmetric with spin; if a gap occurs at E_F for one spin but not the other, the result is a half metal (ex. Co_2MnAl).[4] Half-metals are important for spintronics applications such as spin transistors and non-volatile logic.

$Cr_{1-x}Al_x$, with $x = 0.15 - 0.26$, shows semiconductor-like electronic behavior. Our photoemission study showed a narrow gap or pseudogap in a $Cr_{0.80}Al_{0.20}$ thin film.[5] A maximum resistivity of 3600 $\mu\Omega$-cm occurs in bulk, with a negative temperature coefficient of resistivity.[6,7] In addition, a large Hall coefficient and a small electronic specific heat are observed[6,8], all hallmarks of semiconducting behavior. The maximum resistivity and Hall coefficient and minimum electronic specific heat all occur around $x = 0.25$. $Cr_{1-x}Al_x$ is antiferromagnetic for $x = 0 - 0.50$, with a plateau in the magnetic susceptibility also at $x = 0.25$.[9–11] This suggests an ordered Cr_3Al structure may be responsible.

The nature of any gap in Cr_3Al is currently of interest. The experimental results in the literature are suggestive of either a semimetal or degenerate semiconductor. A full, semiconducting gap might suggest further study of Cr_3Al as a potential thermoelectric material. In addition, recent theoretical work has predicted that Cr_3Al with a binary Heusler ($D0_3$) ordering is almost completely spin polarized and that Mn doped $D0_3$ Cr_3Al would behave as a true half metal with applications in spintronics.[12] While no evidence of $D0_3$ ordering has been shown in Cr_3Al, the Cr-Al phase diagram is not well established. Thus, a study of the nature of a gap in Cr_3Al and how it is affected by chemical ordering is warranted.

Recent work from our group showed that both antiferromagnetism and chemical ordering are necessary for the semiconductor-like behavior in $Cr_{1-x}Al_x$ to occur. Two film samples were presented, both antiferromagnetic, but with different electronic properties. The films were grown at different temperatures so that one was metallic and one nonmetallic, attributed to differences in chemical ordering of Cr and Al on the bcc sublattice.[13] The current paper explores the issue of chemical ordering in Cr_3Al more deeply, with density functional theoretical calculations considering five possible structures with the Cr_3Al stoichiometry, and a systematic study of thin film growth of $Cr_{1-x}Al_x$ varying concentration, growth temperature, and substrate. Our results support the proposed Cr-Al phase diagram and show that $D0_3$ ordering is unlikely to occur. We also show how the antiferromagnetic X-phase structure explains the observed electronic transport behavior and find that a perfect crystal of X-phase Cr_3Al should have a complete band gap.

II. BACKGROUND

The structural Cr-Al phase diagram is not clear. Based on x-ray diffraction (XRD), Koster et al[10] created a phase diagram of $Cr_{1-x}Al_x$ in 1963. Koster's phase diagram, reproduced in Figure 1(a), shows a bcc solid solution (α) as the stable phase from $x = 0 - 0.26$. The $C11_b$ Cr_2Al (β) phase is shown for $x = 0.29$ - 0.34 and a two phase region is shown between $x = 0.26$ - 0.29. Koster et al. suggested that a Cr_3Al ordered compound may exist due to the nonlinear dependence of magnetic susceptibility on x, but found no evidence for it in XRD and did not include it in the phase diagram.

In 1981, den Broeder et al saw evidence in transmission electron microscopy (TEM) diffraction patterns for an ordered Cr_3Al structure at temperatures below 400°C.[14] They observed additional diffraction spots which could be interpreted as superlattice spots. They proposed an ordered phase, called the X-phase, for $x = 0.19$ - 0.26, with a low 400°C phase boundary. The updated phase diagram, taken from Murray's 1998 phase diagram evaluation, is shown in Figure 1(b).[15]

According to dark field imaging, the X-phase ordering occurs in small, 1-3nm domains, even within a large bcc crystallite. The roughly 400°C phase boundary was suggested because annealing at temperatures 400°C or above did not improve the size of the crystallites.[14] Such a low temperature phase boundary can impede long range order because the low atomic mobility requires extremely long annealing times to achieve ordering. Thus, the X-phase observed by den Broeder et al is best described as short- to medium-range order.

Based on first order diffraction spots, the authors suggested that the X-phase was a rhombohedral structure with 8 atoms in the unit cell. Because no higher order diffraction spots were observed, they could not be conclusively attributed to a specific structure and thus Cr_3Al and Cr_5Al_3 were both suggested as candidates for the X-phase. For the purposes of this work, we consider the Cr_3Al structure due to the observed anomalous behavior peaking at $x = 0.25$. The X-phase is still considered speculative because it has only been observed once.

The proposed phase diagram in Figure 1(b) shows, for the Cr_3Al composition, three solid phases occurring in different temperature ranges. The X-phase is stable below 400°C, the $C11_b$ Cr_2Al + bcc Cr two phase system is stable from 400°C to 800°C, and the bcc solid solution is stable above 800°C until melting.

Another structure worthy of consideration is the binary Heusler ($D0_3$) structure. The Heusler structure is commonly seen for compounds with a ratio of transition metal:main group element of 3:1. The Heusler compounds have a standard electronic band structure with a band gap between the twelfth and thirteenth bands, so that compounds with a total number of valence electrons $Z = 24$ are semiconducting or semimetallic (e.g. Fe_2VAl), and many compounds with more or less electrons are predicted to be half metallic (e.g. Co_2MnAl). The semiconductor-like behavior in Cr_3Al is reminiscent of the behavior in Heusler-structure Fe_2VAl, but cannot be explained by the Heusler structure because $Z = 21$ for Cr_3Al. However, theoretically, Heusler Cr_3Al may be desirable as a potential half metal.[12] Although $D0_3$ Cr_3Al does not appear on the currently available Cr-Al phase diagrams, it might be reasonable to expect it to be formed under certain growth conditions.

We will explore here the three structures shown on the proposed phase diagram: bcc solid solution, $C11_b$ Cr_2Al + bcc Cr two-phase system, and X-phase Cr_3Al structure. Also included are an off-stoichiometric $C11_b$ Cr_3Al structure, which we see experimentally for films grown at 500-600°C (above the proposed X-phase transition temperature), and the common $D0_3$ structure.

A. bcc Cr

Cr occurs in the bcc structure, shown in Figure 2(a), and all the Cr_3Al structures discussed here have a bcc-like atomic environment, albeit with different types of chemical ordering and in some cases slight distortion.

The bcc structure has one atom per primitive unit cell. However, when simple antiferromagnetism is considered, there are two atoms per unit cell (one up - cube edge, one down - body center).

B. bcc solid solution $Cr_{0.75}Al_{0.25}$

This structure occurs when Al is added to the bcc Cr system and the Al atoms are placed randomly on the lattice sites. The lattice constant is increased slightly because the atomic radius of Al is larger than that of Cr.[6] This structure is shown in Figure 2(b).

C. $C11_b$ Cr_2Al

The $C11_b$ Cr_2Al structure is layered along the bcc (001) planes, so that there are alternating layers (Cr, Cr, Al, Cr, Cr, Al...). Thus the unit cell consists of essentially three bcc unit cells, with six atoms per Cr_2Al unit cell. The layering creates a 4% tetragonal distortion.[10] The $C11_b$ Cr_2Al structure is shown in Figure 2(c).

The proposed phase diagram only shows single phase $C11_b$ Cr_2Al for about $x = 0.29 - 0.34$, so for the Cr_3Al stoichiometry, the two phase $C11_b$ Cr_2Al + bcc Cr structure is considered. $C11_b$ Cr_2Al also displays simple antiferromagnetism.[16]

D. $C11_b$ Cr_3Al

Although single-phase $C11_b$ does not appear for the Cr_3Al stoichiometry on the phase diagram, we observe it experimentally. In this case, the $C11_b$ Cr_2Al structure has the additional Cr atoms substituted randomly onto Al sites (i.e. $Cr_2(Al_{1-\delta}Cr_\delta)$, where $\delta = 0.25$ for the Cr_3Al stoichiometry). The $C11_b$ Cr_3Al structure is shown in Figure 2(d).

E. $D0_3$ Cr_3Al

We include the binary Heusler structure ($D0_3$), although it does not appear on the phase diagram, because so many other bcc transition metal-Al alloys take this form. The full Heuslers have a A_2BD structure, where A and B are transition metals and D is an *sp* element. The atoms occupy the sites of a bcc lattice with an $L2_1$ ordering. For binary Heuslers (A_3D), atom A occupies two distinct sites and can be thought of as $A(I)_2A(II)D$ (e.g. Fe_3Si).

The $D0_3$ ordering can be seen as 4 interpenetrating fcc lattices, thus the primitive unit cell contains 4 atoms. In Figure 2(e), Cr(I) occupy the body centers of the cube, while Cr(II) and Al occupy alternating cube edges. Cr_3Al in the $D0_3$ structure has been considered theoretically before, and has been calculated to be ferrimagnetic due to antiferromagnetic coupling between the Cr(I) and Cr(II) sites with different magnitudes of moment.[12]

F. X-phase Cr_3Al

The proposed X-phase is a chemically ordered, rhombohedrally distorted phase based on the bcc structure.[14] The primitive unit cell is a rhomboid containing 8 atoms along the bcc [111] direction: 6 Cr atoms followed by 2 Al atoms. The primitive lattice vectors are [211], [121], and [112] in the bcc coordinates. The space group for this structure is $R\bar{3}m$. The rhombohedral unit cell appears in Figure 2(f).

This structure has not been widely observed or studied. Thus, there is no Strukturbericht designation or accepted parent compound for it. We will continue to call it the "X-phase" for the bulk of this paper.

III. EXPERIMENTAL METHODS

Most previous studies of Cr-Al alloys have used bulk samples, although a few studies have focused on the potential applications of Cr-Al thin films as the antiferromagnetic layers in exchange-biased multilayer systems[17–19] and as thin film resistors.[20] In contrast to bulk sample growth, thin film growth often stabilizes nonequilibrium crystal structures, for example through quenching of films grown at high temperatures, restriction of lattice parameters due to the substrate, and surface energy effects. We have used thin film growth techniques in order to study the effect of structure on the transport properties of Cr-Al.

Thin films of $Cr_{1-x}Al_x$, with thickness ∼400Å, were grown on MgO(001) and *a*-SiO_2/Si substrates to achieve epitaxial and polycrystalline growth, respectively. by co-deposition of Cr from an e-beam source and Al from an effusion cell at a rate of 0.4 Å/s and a base pressure of 5×10^{-9} Torr. One series was grown at a substrate temperature of 300°C, with the Al concentration (x) varied. Another series of films was grown at a fixed Al concentration ($x = 0.24$) but varied substrate temperature from 200-600°C. We did not attempt growth above 600°C due to the potential loss of Al above its melting temperature (660°C).

Cr(001) is known to grow epitaxially on MgO(001).[21,22] The MgO lattice constant is 4.211Å, or about $\sqrt{2}$ larger than that of Cr. The Cr lattice grows 45° rotated compared to the substrate ([001]Cr || [110]MgO). For pure Cr, the lattice mismatch for this epitaxial relation is 3.9%, while the addition of Al increases the lattice constant and improves the mismatch to approximately 1% at the Cr_3Al stoichiometry. Epitaxy was verified in-situ by reflection high energy electron diffraction (RHEED) which showed a streaky pattern and ex-situ by x-ray diffraction (XRD) which showed four-fold symmetry of the (011) peak in an azimuthal scan at 45° from normal. In addition, only the bcc (001) orientation is seen in a $\theta - 2\theta$ scan (see Figure 3(a)). The films grown on *a*-SiO_2/Si are polycrystalline, as the *a*-SiO_2 layer provides an amorphous surface for growth. In addition, it acts as a diffusion barrier to prevent silicide formation at the interface.

The films were patterned lithographically to form a defined geometry for the resistivity measurements. The resistivity was measured from 2-300K by a four-probe technique, averaging forward and reverse currents to avoid thermal voltages. In addition, the I-V curve was confirmed to be linear for each sample.

IV. EXPERIMENTAL RESULTS

The 2K resistivity of films as a function of Al concentration is shown in Figure 4. It shows a clear peak at 25 at. % Al, similar to the results on bulk samples.[6,7] In addition, the temperature dependence of the resistivity is shown in the inset for 23 at. % Al for both an epitaxial and polycrystalline film. The negative temperature dependence is decidedly nonmetallic, and similar to what has been seen in bulk.

However, there are significant differences between the thin films and bulk. In the bulk, the metallic Cr_2Al phase begins to precipitate at 26 at. % Al, leading to a steep drop in resistivity above 25 at. %. Thus, it could not be

determined previously whether the peak ρ(2K) at 25 at. % Al was related to formation of a distinct Cr_3Al phase, or whether a peak in ρ(2K) occurred at 25 at. % Al simply due to an accidental confluence of factors: slowly increasing resistivity with x combined with a sudden drop at 26 at. % Al due to precipitation of metallic Cr_2Al.

In contrast to bulk, none of our films shown in Figure 4 (grown at 300°C) show evidence of the Cr_2Al phase in XRD, up to 37 at. % Al. The resistivity of our films still peaks at 25 at. % Al, but the decrease in resistivity for concentrations above 25 at. % is much more gradual in the films than in bulk, still displaying nonmetallic behavior up to about 37 at. % Al. This suggests that the peak in ρ(2K) at 25 at. % Al is not related to precipitation of the Cr_2Al phase, but rather to an ordered Cr_3Al structure.

The magnitude of the peak resistivity reaches about 2400 $\mu\Omega$-cm in the films, but as high as 3600 $\mu\Omega$-cm in the bulk.[6,7] This difference is as of yet unexplained, but could be due to a different quality of Cr_3Al formation in the samples, or due to strain in the films, either from thermal expansion or substrate mismatch effects.

Figure 4 also shows a noticeable effect of the substrate. The polycrystalline films, grown on a-SiO_2/Si, have a significantly lower resistivity than their epitaxial counterparts. This can be seen clearly in the Figure 4 inset comparing two films grown at the same time on different substrates. The polycrystalline films not only have lower 2K resistivity, but a weaker temperature dependence of resistivity.

This result is surprising at the outset, given that the primary quantities leading to the resistivity are the scattering time τ and the number of carriers n. The addition of grain boundaries adds scattering centers and should decrease τ, leading to higher resistivity. The lower resistivity of the polycrystalline samples implies an opposing, and larger, effect on n, further suggesting that the anomalous transport behavior in this material is due to a band structure effect.

A second series of samples, with 24 at. % Al, varied growth temperature between 200-600°C. The 2K resistivity is shown in Figure 5. The results show a transition from clearly nonmetallic behavior at lower growth temperature to more metallic behavior at the highest growth temperatures, as seen in the previous study.[13] This data shows the transition around 400°C, aligning with the proposed phase boundary from X-phase Cr_3Al to metallic $C11_b$ Cr_2Al + Cr (Figure 1). Indeed, the epitaxial films grown at 500 and 600°C show $C11_b$ superlattice peaks at the bcc $(0\ 0\ \frac{2}{3})$ position[23], while the films grown at low temperature do not, as shown in Figure 3(b).

The transition from nonmetallic to metallic behavior is much sharper in the polycrystalline films than the epitaxial films. In addition, the high temperature grown polycrystalline films are much more metallic than the epitaxial ones. The difference in behavior between the epitaxial and polycrystalline films is not exactly clear, but one possibility is due to different formation of the $C11_b$ phase in these films.

Although the proposed Cr-Al phase diagram shows a two phase region of $C11_b$ Cr_2Al + Cr for the Cr_3Al concentration (Figure 1), our XRD data is indicative of a single-phase off-stoichiometric $C11_b$ Cr_3Al ($Cr_2(Al_{1-\delta}Cr_\delta)$) for the epitaxial films grown at 500 and 600°C. The structure is shown in Figure 2(d). This is consistent with the findings for the 600°C grown thick film in the previous study.[13] Figure 3(c) shows that the (0 0 2) peak in XRD does not split as it would in the case of two phase $C11_b$ Cr_2Al + Cr. The position of the (002) peak shifts to the right with increasing growth temperature, due to tetragonal distortion. We also see that c, the axis along which ordering occurs, points preferentially in the out of plane direction. Due to the tetragonal distortion of the $C11_b$ structure, the different a and c lattice constants would also lead to a split diffraction peak if c were randomly oriented throughout the film.

The formation of single-phase $C11_b$ Cr_3Al in our epitaxial films, although it does not occur in the phase diagram, is not surprising. Samples grown using vapor deposition techniques often show nonequilibrium structures, due to the kinetics of phase nucleation. In addition, surface energy effects during growth can cause ordering to occur preferentially along a certain direction, which can explain the orientation of the $C11_b$ c axis in the out of plane direction. Finally, epitaxy may cause one phase to be preferred over another due to a better lattice constant match with the substrate, or preferential orientation due to a constraint on the lattice constant in the in-plane direction.

V. THEORETICAL METHODS

DFT calculations of all structures considered were done using the AkaiKKR code, so that the results for the different structures could be compared directly. AkaiKKR is a full-potential density functional Green's function approach based on the Korringa-Kohn-Rostoker multiple-scattering technique.[24–26] This technique was chosen for its ability to treat site disorder, which was necessary for the bcc solid solution and off-stoichiometric $C11_b$ Cr_3Al structures. Disorder is treated using the coherent potential approximation (CPA).[27,28] The number of irreducible k points used for Brillouin zone integration was between 3009 and 3276 for the different structures. The scalar relativistic approximation was used and the generalized gradient approximation (GGA) was used to approximate the exchange-correlation energy[29].

For the X-phase Cr_3Al structure, additional calculations were done in order to better understand the nature of the pseudogap found in the KKR calculations. These calculations were done using a plane wave pseudopotential code, Quantum Espresso,[30] as well as a full potential linear muffin tin orbital approach (FP-LMTO)[31]. The Perdew-Burke-Erzenhof (PBE) formulation of the generalized gradient approximation was used to describe exchange and

correlation[32]. Ultrasoft pseudopotentials were used for all of the plane wave calculations. For this study, we used the Cr pseudopotential from the study by R. Soulairol *et al.*[33] which we found to provide better results for bulk Cr compared to other available pseudopotentials in the Quantum Espresso distribution, specifically Cr.pbe-sp.van.UPF and Cr.pw91-sp-van.UPF. An energy cutoff of 40 Ryd was used for the plane wave expansion to describe the wavefunctions. The charge density and potential were determined using a 400 Ryd energy cutoff. Brillouin zone sampling was done using a 24x24x24 Monkhorst-Pack grid. The general parameters (exchange-correlation, k-point mesh) were identical for the FP-LMTO calculations. Angular momentum channels up to $l = 3$ were included in the FP-LMTO calculations. The tetrahedron approach was used to calculate the density of states in the FP-LMTO calculation. The plane wave pseudopotential density of states calculation used a Methfessel-Paxton smearing energy of 68 meV.

VI. THEORETICAL RESULTS

Because pure Cr is a well studied system, we compare our calculations of Cr to experiment to verify that we have chosen appropriate parameters. The calculated Cr lattice constant is very close to experiment (2.882Å calculated, 2.885Å experimental). In addition, the bulk modulus is extremely close (1.86 Mbar calculated, 1.97 Mbar experimental). Pure Cr has a spin density wave (SDW) incommensurate with the lattice that is computationally difficult. Not only does it require a large unit cell but it is, as of yet, not found to be the minimum energy state in current DFT calculations.[34] For these reasons, we simplify and assume the commensurate SDW (simple antiferromagnetism) for Cr. We obtain a larger magnetic moment than experimentally observed (1.1 μ_B calculated, 0.60 μ_B experiment[9], in the commensurate SDW phase). The large calculated Cr moment is consistent with calculations in the literature and is due to overestimation of the moment by the GGA approximation.[34]

Table I shows the relevant calculated parameters for the Cr_3Al structures. The first and second columns show the lattice parameters and magnetic state. Both the calculated bcc solid solution and X-phase have similar lattice parameters to experiment. The rhombohedral distortion of the X-phase is small, and if it occurred in many small domains as seen experimentally by den Broeder[14], the distortion would not be seen in XRD. The Cr_2Al phase, on the other hand, has a significant tetragonal distortion, which is seen experimentally.[23] The $D0_3$ phase has cubic symmetry, but a significantly larger lattice constant than the experimental value. All of the calculated structures show antiferromagnetic order except $D0_3$, which shows ferrimagnetism. This is consistent with previous calculations[12] and the well-known Heusler Slater-Pauling behavior.[35] Further details of the magnetic configurations, including magnetic moments on the Cr atoms, have been given previously.[13] Thus, the Cr_3Al experimental data are not consistent with the $D0_3$ structure.

The total energy per atom, relative to the minimum energy system, is shown in the third column. The X-phase structure has the lowest energy, suggesting that it is the low temperature stable phase for the Cr_3Al stoichiometry, as suggested in the proposed phase diagram (Figure 1(b)). The bcc solid solution, $C11_b$ Cr_2Al + bcc Cr two phase system, and $C11_b$ Cr_3Al structure have the next lowest energies, consistent with their being stable phases at higher temperatures. Finally, the $D0_3$ structure has a significantly higher energy.

The bcc solid solution, $C11_b$ Cr_3Al, and the $C11_b$ Cr_2Al + bcc Cr two phase system have some degree of disorder. This suggests that entropy of mixing drives the transition from the Cr_3Al X-phase. The energy difference between the X-phase Cr_3Al structure and the bcc solid solution is about 0.042 eV. In a model including only entropy of mixing, the order-disorder transition between these two structures should be about 600°C, within the range of the transition on the proposed phase diagram. The $C11_b$ systems are more difficult to model because of the lattice distortion and, in the case of the two phase system, the temperature-dependent solubility of Al in Cr and in $C11_b$ Cr_2Al. The $D0_3$ structure has no more disorder than the X-phase structure and therefore should theoretically never occur in the equilibrium phase diagram based on energy or entropy.

The fourth column in Table I shows the density of states (DOS) at E_F. It should be noted that because Cr and the Cr-Al alloys have a pseudogap at E_F due to the antiferromagnetism, the DOS is sharply varying near E_F and the exact value for DOS(E_F) depends somewhat on the input parameters of the calculation. The DOS curves have been shown previously.[13]

To compare the calculated values of DOS(E_F) to experimental values, we adjust experimental values for the Sommerfeld coefficient (γ) from the literature by the factor $(1 + \lambda)$. We used $\lambda = 0.34$, one of the reported values for Cr. This value was calculated based on the Sommerfeld coefficient from specific heat measurements and a previously accepted value for the DOS(E_F).[36–40] This is a fairly typical value for λ in the transition metals, however, reported values for λ in Cr vary.[41–43] No values of λ have been reported for Cr_3Al.

Our calculated DOS(E_F) for Cr is lower than the experimental value by 15%, showing the approximate level of error in DOS(E_F) calculations. X-phase Cr_3Al has the lowest DOS(E_F) by more than a factor of two, closest to the experimental value based on the Sommerfeld coefficient for Cr_3Al.

The decreased DOS(E_F) in X-phase Cr_3Al is due to a semimetallic band structure, as calculated by KKR. The full

band structure has been shown previously,[13] and a closeup of the region around E_F is shown in Figure 6(e). Figure 6 shows the evolution of the band structure from Cr to Cr_3Al as X-phase ordering and antiferromagnetism are added to the calculation.

Figure 6(a) shows the band structure of pure, nonmagnetic Cr, which is well known.[44] Figure 6(b) shows how this same band structure appears when plotted in the rhombohedral zone used for X-phase Cr_3Al. The DOS, shown to the right of each band structure, is of course identical. The antiferromagnetic pseudogap in Cr occurs where the bands cross at $\Gamma - M$ and $\Gamma - R$, and at one of the crossings in $\Gamma - X$ in the cubic zone. In the rhombohedral zone, this corresponds to gaps at the band crossings at $\Gamma - L$ and $\Gamma - T$, and one of the band crossings at each of $\Gamma - F$ and $T - F$ (Figure 6(c)). This leaves bands still crossing E_F around the F point, allowing significant electronic transport and metallic behavior, as expected for Cr.

In nonmagnetic X-phase Cr_3Al, shown in Figure 6(d), significant band hybridization is seen compared to Cr. The addition of antiferromagnetism, shown in Figure 6(e), shifts the bands farther apart, leaving bands crossing E_F only slightly at the F and T points. This results in a very low DOS and pseudogap, shown in the panel to the right.

The mechanism for the opening of the antiferromagnetic pseudogap is different in Cr and Cr_3Al. In Cr, the antiferromagnetism doubles the unit cell from one atom (bcc) to two atoms (one up, one down, in a simple cubic unit cell). Thus, the band structure in the bcc zone is folded into the cubic zone, and where the bands cross, they open up to form a gap.[44] In X-phase Cr_3Al, the unit cell is the same for the nonmagnetic and antiferromagnetic case (8 atoms or Cr_6Al_2, see Figure 2(f)). The band structure responsible for the pseudogap is already apparent in nonmagnetic X-phase Cr_3Al, although the DOS(E_F) is still quite large. The addition of antiferromagnetism simply pushes the valence and conduction bands further apart, so that the band edges are very close to E_F, and thus lowers the total energy of the system.

Despite the different mechanisms, the result of antiferromagnetism is similar in Cr_3Al and Cr. In both cases, the antiferromagnetism eliminates bands crossing E_F along $\Gamma - F$, $\Gamma - L$, and $\Gamma - T$. The X-phase ordering in Cr_3Al hybridizes the bands so that very few states (if any) appear at E_F around F and T. The combination of antiferromagnetism and X-phase ordering results in the observed semimetallic band structure and very low DOS(E_F) from KKR calculations.

Density functional calculations often underestimate the band gap in materials, sometimes showing overlapping bands even in materials known to have a full band gap[45]. The density of states calculated using the KKR approach shows a small finite density of states at the Fermi energy, indicating a semimetal. Since very little experimental or theoretical work has been done on the X-phase of Cr_3Al, we also performed complementary calculations using both a plane wave approach (Quantum Espresso) as well as a full potential linear muffin tin orbital approach (FP-LMTO).

Figure 7 compares the calculated DOS for the three approaches. It is clear that, overall, the different theoretical approaches are in good agreement and produce similar features in the DOS near the Fermi energy. The Quantum Espresso calculations predict a small but complete gap of 200 meV and valence bands that are shifted to lower energy compared to the KKR and FP-LMTO approaches. The FP-LMTO density of states calculations also reveal a band gap, albeit a smaller one of 40 meV.

The discrepancy between the different approaches on the presence and size of the band gap could be due to several factors. Ultrasoft pseudopotentials are known to overestimate the magnetization energy in transition metals and this error is generally larger when the generalized gradient approximation is used[46]. Both the KKR and FP-LMTO techniques are all-electron approaches so they avoid this problem. Another source of error could come from the calculation of the density of states in the KKR framework. The density of states in this case can be expressed in terms of the system Green's function as:

$$n(E) = \lim_{\eta \to 0^+} \left[-\frac{1}{\pi} \mathrm{Im} G(E + i\eta) \right] \tag{1}$$

due to the fact that the Green's function is analytic everywhere in the complex plane except the real axis. In practical calculations, we add a small imaginary component, η, to the energy. This imaginary component leads to an artificial broadening of the density of states which can be expressed as a Lorentzian with a half-width of η. For the calculations shown in Fig. 7, an imaginary component of 1 meV was used. Broadening due to this source would be insufficient to explain the entire difference between the KKR and FP-LMTO results. However, given that density functional calculations underestimate the experimental band gap, it is reasonable to assume that a perfect X-phase Cr_3Al crystal would be a small band gap semiconductor.

VII. DISCUSSION

Thus, the semiconductor-like behavior in Cr_3Al can be explained by X-phase type chemical ordering and antiferromagnetism leading to a gap in the DOS. It is likely that a perfect crystal of X-phase Cr_3Al would be a true narrow-gap semiconductor with a band gap greater than 40 meV. Experimental estimations of the gap energy range from 10-95 meV.[5,6,47,48] However, real samples thus far show the X-phase occurring in very small domains presumably separated by anti-phase boundaries.[14] This disorder could smear the band edges or introduce defect states.[49] The experimental observations of Cr_3Al are consistent with a small but finite DOS(E_F): the electronic contribution to the specific heat is nonzero, and the electrical resistivity increases with decreasing temperature algebraically rather than exponentially. This indicates either a semimetal (slightly overlapping flat bands at E_F) or a degenerate semiconductor (E_F just inside the band edge). The negative dependence of resistivity on temperature is most likely due to localization phenomenon or a rapidly varying DOS(E_F), rather than true activated behavior.

A band gap can only occur in a material with an even number of valence electrons per unit cell in order to completely fill the valence band. So how can Cr_3Al, with 21 electrons per formula unit, have a band gap? The gap is possible because the primitive unit cell of the X-phase, shown in Figure 2(f), is actually Cr_6Al_2, with a total of 42 valence electrons per unit cell. This aspect of the X-phase structure sets it apart from the other structures, which, although they may have a low DOS(E_F), have an odd number of valence electrons per unit cell and therefore *must* have partially filled bands crossing E_F.

This study of the possible types of chemical ordering of Cr_3Al on the bcc lattice has important implications for materials design of transition metal compounds. It is clear from the calculated lattice constant and ferrimagnetic character of $D0_3$ Cr_3Al that the bulk samples reported in the literature and the thin film samples reported here do not occur in the $D0_3$ structure. The energy calculations show that the $D0_3$ structure should not occur at all under equilibrium conditions. However, as has been seen in this paper with regard to $C11_b$ Cr_3Al, nonequilibrium structures may occur for thin film growth due to kinetics, surface energy effects, or epitaxy. Because there are four other structures that are favored energetically (and in some cases, entropically), it seems unlikely that the $D0_3$ structure could be formed. However, if $D0_3$ Cr_3Al were desired, for example for study as a possible half metal,[12] one direction of research would be to take advantage of the difference in lattice constant and grow ultrathin epitaxial films. The calculated $D0_3$ Cr_3Al lattice constant actually has an exceptionally good lattice match to MgO (0.1%), but has not appeared in any of the 400Å thin films on MgO reported here. Growth of an ultrathin (unrelaxed) film may have more potential.

The Heusler structure ($D0_3$ for binary and $L2_1$ for ternary compounds) is fairly common, occuring for hundreds of transition metal-main group compounds. Cr_3Al, with X-phase ordering as the equilibrium state, is an exception to this scheme. This may represent a lower limit on the number of valence electrons in the unit cell for the Heusler structure to form. There are 21 valence electrons in the formula unit of Cr_3Al, while Heusler alloys are usually studied in the range 22-31 valence electrons.[35] Thus, similar compounds containing transition metals from the left side of the periodic table should be studied for X-phase type ordering like that seen in Cr_3Al.

VIII. CONCLUSION

In summary, we used both experimental thin film growth methods and theoretical DFT calculations to show how a combination of antiferromagnetism and X-phase chemical ordering lead to a gap in the band structure of Cr_3Al. Our experimental data correlates a transition from nonmetallic to metallic transport behavior around 400°C growth temperature with the previously proposed structural phase transition (X-phase $\rightarrow$ $C11_b$) occurring around the same temperature. Theoretically, the proposed X-phase is found to be the lowest energy structure of those considered, implying it should be the equilibrium structure occurring in nature. The commonly seen $D0_3$ (Heusler) structure is not observed, and based on calculations of total energy, is unlikely to occur.

ACKNOWLEDGMENTS

This work was supported by the U.S. Department of Energy under Contract No. DE-AC02-05CH11231. Calculations were done at the Cornell Nanoscale Facility, part of the National Nanotechnology Infrastructure Network (NNIN) funded by the NSF. The authors would like to thank H. Akai for advice and insight on the AkaiKKR calculations, Mark van Schilfgaarde for advice on the FP-LMTO calculations, and Cyrille Barreteau for providing the ultrasoft Cr pseudopotential used in this work.

* Email: zboekelheide@berkeley.edu; Present address: Material Measurement Laboratory, National Institute of Standards and Technology, Gaithersburg, Maryland 20899, USA

[1] M. Weinert and R. E. Watson, Phys. Rev. B **58**, 9732 (1998).
[2] C. Uher, J. Yang, S. Hu, D. T. Morelli, and G. P. Meisner, Phys. Rev. B **59**, 8615 (1999).
[3] J. O. Sofo and G. D. Mahan, Phys. Rev. B **49**, 4565 (1994).
[4] J. Kübler, A. R. Williams, and C. B. Sommers, Phys. Rev. B **28**, 1745 (1983).
[5] Z. Boekelheide, A. X. Gray, C. Papp, B. Balke, D. A. Stewart, S. Ueda, K. Kobayashi, F. Hellman, and C. S. Fadley, Phys. Rev. Lett. **105**, 236404 (2010).
[6] D. J. Chakrabarti and P. A. Beck, J. Phys. Chem. Solids **32**, 1609 (1971).
[7] L. V. Nomerovannaya and V. A. Rassokhin, Phys. Status Solidi A **79**, 87 (1983).
[8] N. Pessall, K. P. Gupta, C. H. Cheng, and P. A. Beck, J. Phys. Chem. Solids **25**, 993 (1964).
[9] E. Fawcett, H. L. Alberts, V. Y. Galkin, D. R. Noakes, and J. V. Yakhmi, Rev. Mod. Phys. **66**, 25 (1994).
[10] W. Koster, E. Wachtel, and K. Grube, Z. Metallkd. **54**, 393 (1963).
[11] A. Kallel and F. deBergevin, Solid State Comm. **5**, 955 (1967).
[12] J. Li, H. Chen, Y. Li, Y. Xiao, and Z. Li, J. Appl. Phys. **105**, 083717 (2009).
[13] Z. Boekelheide, T. Saerbeck, A. P. J. Stampfl, R. A. Robinson, D. A. Stewart, and F. Hellman, Physical Review B **85**, 094413 (2012).
[14] F. J. A. den Broeder, G. van Tendeloo, S. Amelinckx, J. Hornstra, R. de Ridder, J. van Landuyt, and H. J. van Daal, Phys. Stat. Sol. (a) **67**, 233 (1981).
[15] J. L. Murray, J. Phase Equilib. **19**, 367 (1998).
[16] M. Atoji, J. Chem. Phys. **43**, 222 (1965).
[17] T. J. Klemmer, V. R. Inturi, M. K. Minor, and J. A. Barnard, Appl. Phys. Lett. **70**, 2915 (1997).
[18] S. M. Zhou, K. Liu, and C. L. Chien, J. Appl. Phys. **87**, 6659 (2000).
[19] C. G. Lee, B. S. Kim, and K. Fukamichi, IEEE Transactions on Magnetics **35**, 2928 (1999).
[20] P. J. Ozawa, S. Yoshizaki, S. Takeyama, T. Enjo, and K. Ikeuchi, IEEE T. Compon. Hybr. **CHMT-9**, 391 (1986).
[21] E. E. Fullerton, S. D. Bader, and J. L. Robertson, Physical Review Letters **77**, 1382 (1996).
[22] E. E. Fullerton, K. T. Riggs, C. H. Sowers, S. D. Bader, and A. Berger, Physical Review Letters **75**, 330 (1995).
[23] E. V. Kozlov, B. S. Semukhin, L. M. Rubinovich, and D. M. Shtern, Fiz. metal. metalloved. **56**, 547 (1983).
[24] Http://sham.phys.sci.osaka-u.ac.jp/kkr/.
[25] J. Korringa, Physica **13**, 392 (1947).
[26] W. Kohn and N. Rostoker, Phys. Rev. **94**, 1111 (1954).
[27] P. Soven, Phys. Rev. **156**, 809 (1967).
[28] H. Akai, J. Phys.: Condens. Matter **1**, 8045 (1989).
[29] J. P. Perdew, J. A. Chevary, S. H. Vosko, K. A. Jackson, M. R. Pederson, D. J. Singh, and C. Fiolhais, Phys. Rev. B **46**, 6671 (1992).
[30] P. Giannozzi and et al, J. Phys. Condens. Matter **21**, 395502 (2009).
[31] M. Methfessel, M. van Schilfgaarde, and R. A. Casali, "Electronic structure and physical properties of solids: The uses of the lmto method," (Springer-Verlag, Berlin, 2000) Chap. A full-potential LMTO method based on smooth Hankel functions.
[32] J. P. Perdew, K. Burke, and M. Ernzerhof, Phys. Rev. Lett. **77**, 3865 (1996).
[33] R. Soulairol, C.-C. Fu, and C. Barreteau, J. Phys.: Condens. Matter **22**, 295502 (2010).
[34] R. Hafner, D. Spišák, R. Lorenz, and J. Hafner, Phys. Rev. B **65**, 184432 (2002).
[35] I. Galanakis, K. Özdoğan, E. Şaşioğlu, and B. Aktaş, Phys. Status Solidi A **205**, 1036 (2008).
[36] D. W. Cooke, Z. Boekelheide, D. R. Queen, and F. Hellman, J. Appl. Phys. **105**, 07C314 (2009).
[37] D. W. Cooke, *Thermodynamic Measurements of Applied Magnetic Materials*, Ph.D. thesis, University of California -Berkeley (2010).
[38] F. Heiniger, E. Bucher, and J. Muller, Phys. Kondens. Mater. **5**, 243 (1966).
[39] D. G. Laurent, J. Callaway, J. L. Fry, and N. E. Brener, Physical Review B **23**, 4977 (1981).
[40] J. F. Goff, Physical Review B **4**, 1121 (1971).
[41] W. L. McMillan, Phys. Rev. **167**, 331 (1968).
[42] S. D. Brorson, A. Kazeroonian, J. S. Moodera, D. W. Face, T. K. Cheng, E. P. Ippen, M. S. Dresselhaus, and G. Dresselhaus, Phys. Rev. Lett. **64**, 2172 (1990).
[43] P. B. Allen, Phys. Rev. B **36**, 2920 (1987).
[44] E. Fawcett, Rev. Mod. Phys. **60**, 209 (1988).
[45] R. M. Martin, *Electronic Structure: Basic Theory and Practical Methods* (Cambridge Press, 2005).
[46] G. Kresse and D. Joubert, Phys. Rev. B **59**, 1758 (1999).
[47] M. A. Lind and J. L. Stanford, J. Phys. Soc. Jpn. **53**, 4029 (1984).
[48] Our photoemission study showed the valence band edge 95 meV below E_F, measured at room temperature. For comparison, the DFT calculations are made at 0 K.
[49] D. I. Bilc and P. Ghosez, Phys. Rev. B **83**, 205204 (2011).
[50] W. Koster, E. Wachtel, and K. Grube, ASM Alloy Phase Diagrams Center P. Villars, editor-in-chief; H. Okamoto and K. Cenzual, section editors; http://www1.asminternational.org/AsmEnterprise/APD, ASM International, Materials Park, OH,

2006.
[51] J. L. Murray, ASM Alloy Phase Diagrams Center P. Villars, editor-in-chief; H. Okamoto and K. Cenzual, section editors; http://www1.asminternational.org/AsmEnterprise/APD, ASM International, Materials Park, OH, 2006.

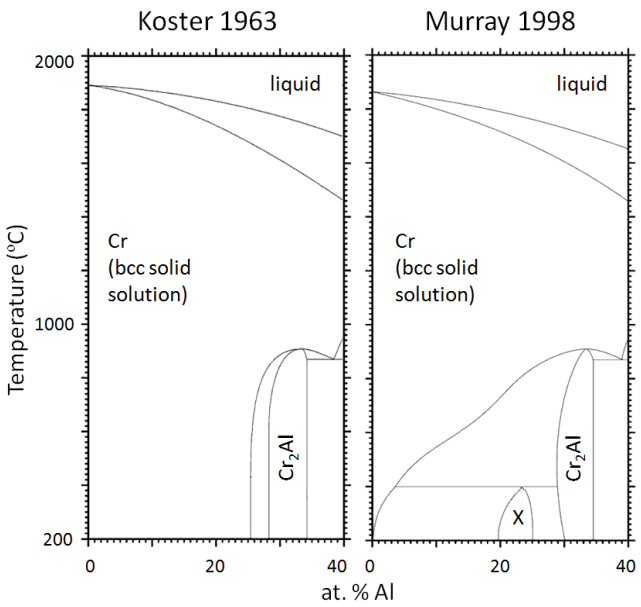

FIG. 1. Binary phase diagrams of the $Cr_{1-x}Al_x$ system, as shown by Koster et al[10,50] and Murray[15,51]. Adapted with permission of ASM International. All rights reserved. www.asminternational.org

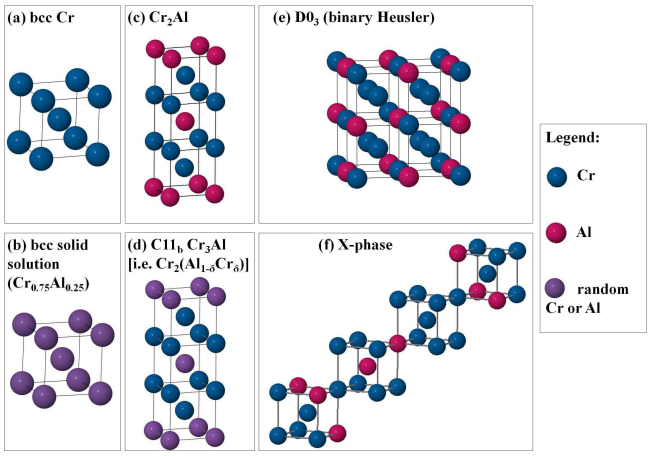

FIG. 2. Structures considered in Sections V and VI. For (b), the atoms are randomly Cr or Al in the ratio $Cr_{0.75}Al_{0.25}$. For (d), the atoms on the Al sites are randomly Cr or Al in the ratio $Cr_{0.25}Al_{0.75}$, for a total stoichiometry of $Cr_2(Al_{0.75}Cr_{0.25})$, or Cr_3Al.

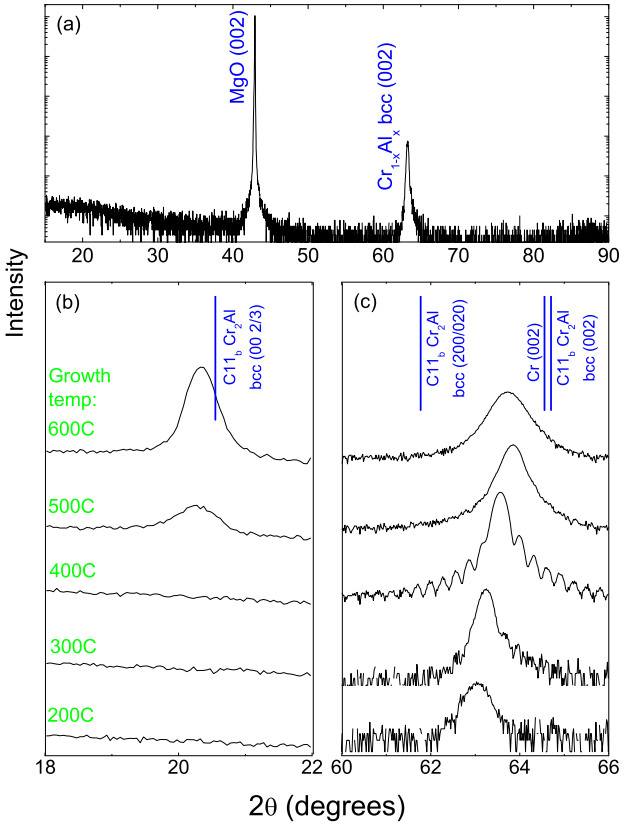

FIG. 3. XRD of epitaxial $Cr_{0.76}Al_{0.24}$ (a) θ-2θ survey of film grown at 300°C. (b) $(0\ 0\ \frac{2}{3})$ peak of films grown at several temperatures. (c) (0 0 2) peak of films for several growth temperatures. Note that some of the (002) peaks have sufficient intensity to show thickness oscillations, corresponding to the approximately 400Å thickness of the films.

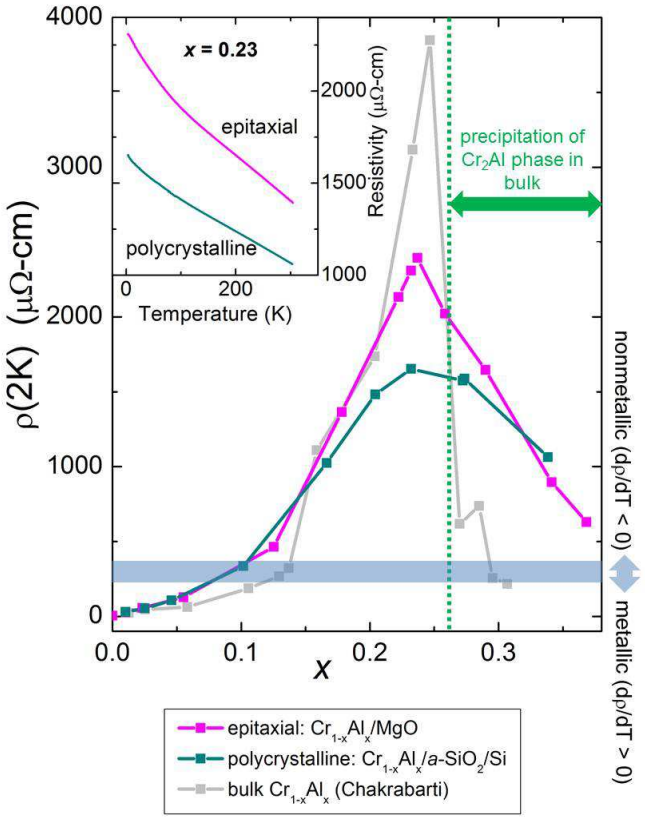

FIG. 4. Resistivity of $Cr_{1-x}Al_x$ thin films vs. x at 2 K. All films shown here were grown at 300°C. Bulk data from Ref. [6]. Error bars are smaller than the symbol size. Inset: Resistivity of $Cr_{0.77}Al_{0.23}$ vs. temperature

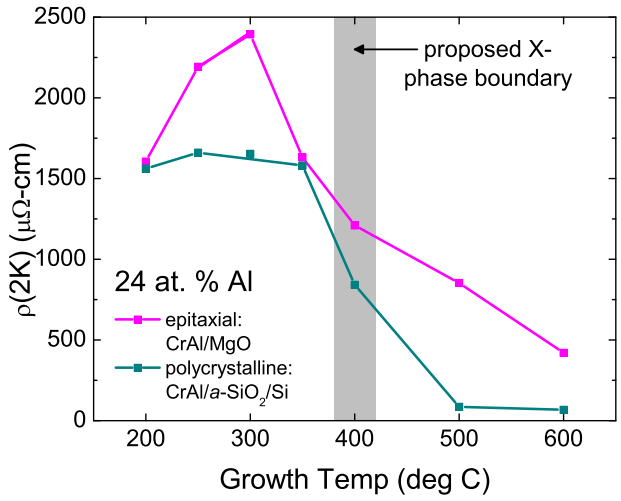

FIG. 5. 2K resistivity of $Cr_{0.76}Al_{0.24}$ thin films vs. growth temperature. Error bars are smaller than the symbol size. The X-phase boundary at 400°C was proposed by den Broeder et al in Ref. [14].

	lattice constants (Å)	Magnetic state	ΔE/atom (eV)	DOS(E_F) (1/eV)
Cr:				
Experiment	$a = b = c = 2.885$Å	antiferromag[44]	–	0.444[8]
Calculated	$a = b = c = 2.882$Å	antiferromag	–	0.379
Cr_3Al:				
Experiment	$a = b = c = 2.949$Å[6]	antiferromag[11]	–	0.108[8]
Calculated				
• bcc solid solut. $Cr_{0.75}Al_{0.25}$	$a = b = c = 2.948$Å	antiferromag	0.042	0.240
• $C11_b$ Cr_2Al + bcc Cr	Cr_2Al: $a = b = 3.017$Å, $c = 2.899$Å; Cr: $a = 2.882$Å	antiferromag	0.039	0.192
• $C11_b$ Cr_3Al	$a = b = 2.979$ Å, $c = 2.915$Å	antiferromag	0.048	0.224
• $D0_3$ Cr_3Al	$a = b = c = 2.977$Å	ferrimag	0.075	0.207
• X-phase Cr_3Al	$a = b = c = 2.941$Å, 90.35° rhomb. distortion	antiferromag	0.000	0.076

TABLE I. Parameters for the five Cr_3Al structures and Cr, as calculated using the KKR technique, and compared to experiment. ΔE/atom is shown relative to the minimum energy structure (X-phase Cr_3Al). The DOS(E_F) is shown per atom. The DOS(E_F)/atom for the two-phase $C11_b$ Cr_2Al + Cr structure is the weighted average of the DOS(E_F)/atom of the two structures.

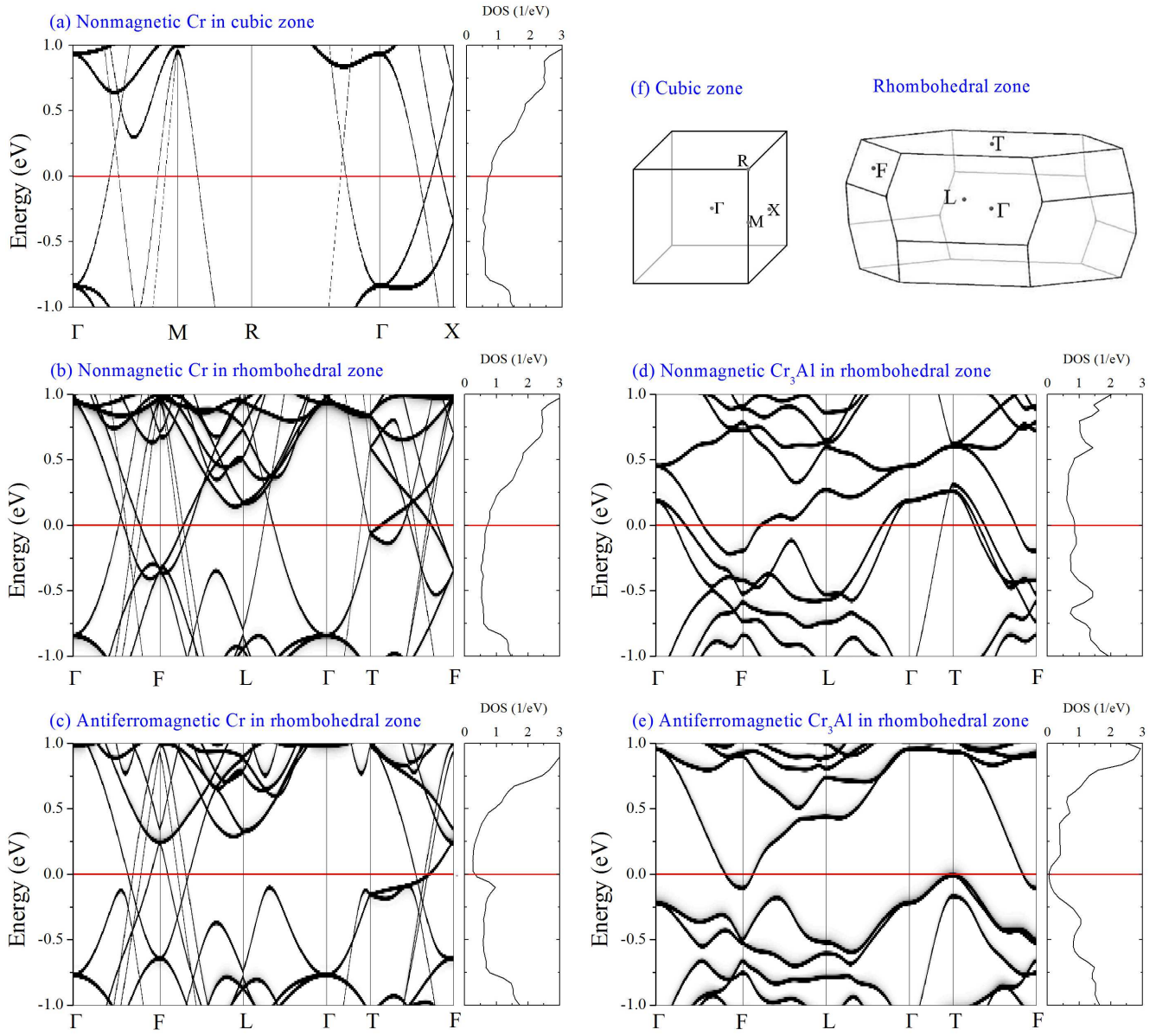

FIG. 6. Band structure of Cr and X-phase Cr_3Al, for nonmagnetic and antiferromagnetic cases, calculated using the AkaiKKR technique. (a) Nonmagnetic Cr in the cubic Brillouin zone; (b) nonmagnetic Cr, (c) antiferromagnetic Cr, (d) nonmagnetic X-phase Cr_3Al, and (e) antiferromagnetic X-phase Cr_3Al, all in the rhombohedral Brillouin zone. (f) Cubic and rhombohedral zones and symmetry points. For reference, point T occurs along the bcc [111] axis (the long axis of the rhomboid unit cell in real space).

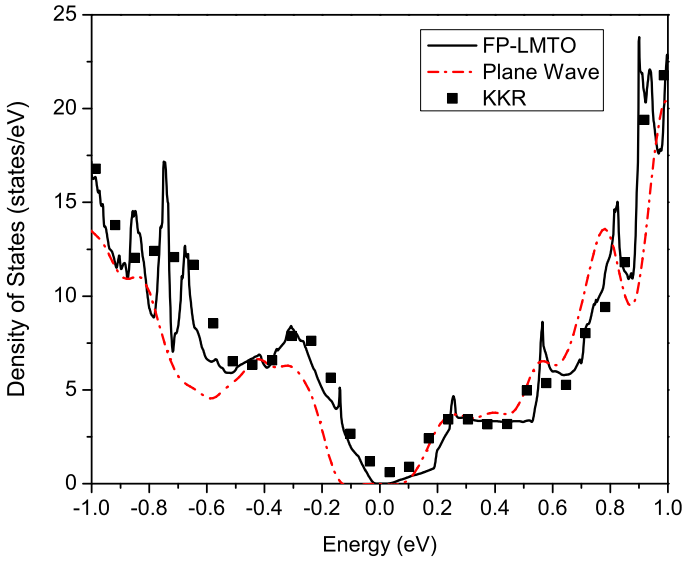

FIG. 7. The total density of states for the X-phase of Cr_3Al is shown as calculated using a FP-LMTO approach (black line), plane wave pseudopotential approach (red line), and the KKR technique (black squares). The energy zero is set to the Fermi energy in all cases.